Boletim da Sociedade Astronômica Brasileira, **37**, no. 1, 5-9

Modeling and MHD simulations of relativistic jets

Understanding complex radio galaxy morphologies

A. S. R. Antas[1] & A. Caproni[2]

[1] Centro Universitário Adventista de São Paulo e-mail: abraao.rodrigues@acad.unasp.edu.br
[2] Universidade Cidade de São Paulo e-mail: anderson.caproni@cruzeirodosul.edu.br

Abstract. This work presents a methodology for analyzing the complex dynamics of jets in radio galaxies through magnetohydrodynamic (MHD) simulations. By focusing on the fundamental physical mechanisms governing the formation, evolution, and interaction of these jets with the intergalactic medium, we aim to bridge the gap between observational phenomena and theoretical models. This comprehensive review covers the derivation of conservative MHD equations, the role of magnetic fields in jet dynamics, and the impact of host galaxy environments on jet morphology. We also consider the environmental characteristics of host galaxies and their relationship with the morphological dichotomies between FRI and FRII objects. Our simulations provide valuable insights into the generation of observed radio structures such as jets, lobes, and plumes, helping to elucidate observational phenomena and contributing to the development of more accurate theoretical models. This study aims to deepen our understanding of the physics of radio galaxies, directly impacting areas such as extragalactic astrophysics, plasma physics, and cosmology.

Resumo. Este trabalho apresenta uma metodologia para analisar a dinâmica complexa de jatos em radiogaláxias por meio de simulações magnetohidrodinâmicas (MHD). Ao focar nos mecanismos físicos fundamentais que governam a formação, evolução e interação desses jatos com o meio intergaláctico, buscamos preencher a lacuna entre os fenômenos observacionais e os modelos teóricos. Esta revisão abrangente cobre a derivação de equações MHD conservativas, o papel dos campos magnéticos na dinâmica dos jatos e o impacto do ambiente da galáxia hospedeira na morfologia dos jatos. Também consideramos as características ambientais das galáxias hospedeiras e sua relação com as dicotomias morfológicas entre objetos FRI e FRII. Nossas simulações fornecem informações valiosas sobre a geração de estruturas de rádio observadas, como jatos, lóbulos e plumas, ajudando a elucidar fenômenos observacionais e contribuindo para o desenvolvimento de modelos teóricos mais precisos. Este estudo visa aprofundar nossa compreensão da física das radiogaláxias, impactando diretamente áreas como astrofísica extragaláctica, física de plasmas e cosmologia.

Keywords. Galaxies: jets – Magnetohydrodynamics (MHD) – Galaxies: active

1. Introduction

The first observations of quasars and the realization of their extragalactic nature Schmidt (1963) immediately suggested the existence of extremely compact and powerful energy sources. Accretion of interstellar gas onto a supermassive black hole was soon identified as the only viable mechanism capable of sustaining such luminosities Salpeter (1964), giving rise to the concept of Active Galactic Nuclei (AGNs). Radio galaxies, quasars, and Seyfert galaxies are among the main classes of AGNs.

Accreting systems are known to generate different types of outflows, among which collimated jets are of particular interest. Large-scale magnetic fields play a central role in powering these structures, either by extracting rotational energy from the black hole via the Blandford–Znajek mechanism Blandford & Znajek (1977) or from the accretion disk through the Blandford–Payne process Blandford & Payne (1982). AGN jets can extend from the vicinity of the event horizon to the intergalactic environment. In the standard scenario Netzer (2015); Urry & Padovani (1995); Antonucci (1993), a rotating supermassive black hole threaded by magnetic fields supplied by the disk continuously winds these initially poloidal fields into toroidal loops, generating the magnetic pressure responsible for jet launching and collimation Tchekhovskoy (2015).

Modeling such jets is intrinsically difficult due to their nonlinear, three-dimensional nature and to the uncertainties related to the disk–jet connection and environmental interactions. While analytical approaches remain valuable, they are limited in capturing the coupled dynamics of radiation, plasma, and magnetic fields. This complexity has driven the increasing reliance on numerical magnetohydrodynamic (MHD) simulations, which provide a controlled framework for investigating jet formation and evolution.

Given these constraints, MHD simulations have become essential tools for probing the physical conditions that shape radio-loud AGN jets. They enable the exploration of regimes inaccessible to analytical models and offer a bridge between theoretical expectations and observations, including the reproduction of large-scale radio structures such as lobes and hotspots. In this paper, we outline the fundamental methodology behind MHD simulations of extragalactic jets, emphasizing the physical principles and computational strategies used to investigate their dynamics and morphology.

2. Radio-Loud AGN

The emission of radio-loud active galaxies is synchrotron in nature. This implies that the radio-emitting plasma contains at least electrons with relativistic velocities (Lorentz factor of the order of $\sim 10^4$) and magnetic fields. Since the plasma must be neutral, it must also contain positive charges. There is no way to determine the particle content directly from synchrotron radiation observations Burbidge (1956).

Fanaroff & Riley (1974) first noted that the relative positions of the high and low surface brightness regions in the lobes of radio galaxy sources are correlated with their radio luminosity. This conclusion was based on a set of 57 radio galaxies and quasars from the complete 3CR catalog, which were resolved at

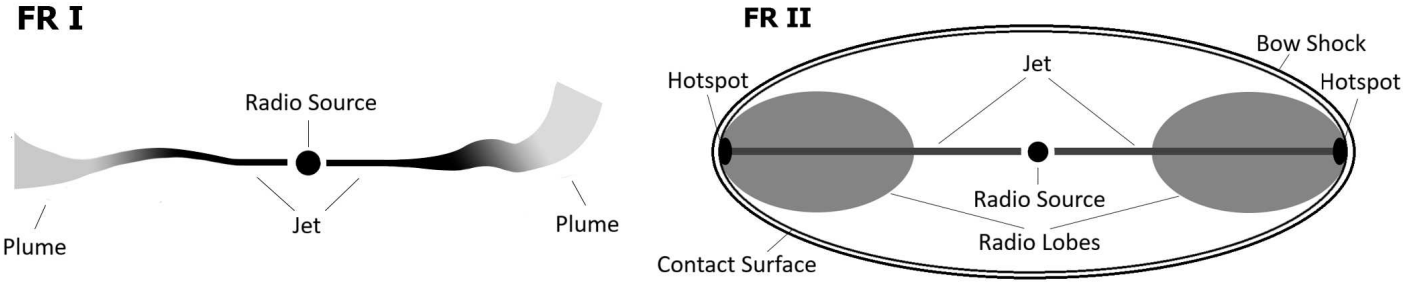

Figure 1. Descriptive scheme for FR I and FR II radio structures.

1.4 GHz or 5 GHz into two or more components. Fanaroff and Riley divided this sample into two classes using the ratio R_{FR} of the distance between the regions of highest surface brightness on opposite sides of the central galaxy or quasar to the total extent of the source (the lowest brightness contour on the map). Sources with $R_{FR} < 0.5$ were placed in Class I and sources with $R_{FR} > 0.5$ in Class II. It was found that almost all sources with luminosity $L(178\ \mathrm{MHz}) \lesssim 2 \times 10^{25} h_{100}^{-2}$ W Hz^{-1} sr^{-1} were Class I, while the brighter sources were almost all Class II. The luminosity boundary between them is not very sharp, and there is some overlap in the luminosities of sources classified as FR-I or FR-II based on their structure. For a spectral index of $\alpha \simeq 1$, the dividing luminosity at 5 GHz is $L(5\ \mathrm{GHz}) \lesssim 7 \times 10^{23} h_{100}^{-2}$ W Hz^{-1} sr^{-1}.

The most common large-scale structures are called lobes: approximately ellipsoidal structures positioned on both sides of the active nucleus, in some cases (FR II radio galaxies) featuring bright hotspots at their extremities, as shown schematically in Figure 1. A significant fraction of low-luminosity sources (FR I radio galaxies) exhibit more elongated structures generally known as plumes (see Figure 1). Some radio galaxies show one or two long and narrow structures known as jets coming directly from the nucleus and extending to the lobes. Since the 1970s, the most widely accepted model Scheuer (1974) has been that the lobes or plumes are powered by beams of high-energy particles and magnetic fields coming from near the active nucleus. Jets are believed to be the visible manifestations of these beams, and often the term jet is used to refer to both the observable feature and the underlying flow.

3. Magneto-Hydrodynamic Theory

The MHD theory describes the dynamics of a fluid under the influence of a magnetic field. To model plasma as a fluid, we need to make the following considerations:

- Condition of quasi-electrical neutrality: The density of negative charges n_e is approximately equal to the density of positive charges n_p.
- Plasma mass condition: The mass density of the plasma is defined as $\rho = n_p m_p$, which is a reasonable approximation since $m_e \ll m_p$ (where m_e is the mass of the electron), characterizing a high density of positive charges and, therefore, a low-frequency plasma.
- Fluid condition: The variations of local thermodynamic quantities are very slow compared to the timescale of microscopic processes in the plasma.
- Generalized Ohm's law: Terms associated with the Hall effect, which allows for the separate movement of ions and electrons, and the inertia of electrons are neglected, ensuring the model's validity only for low-frequency phenomena and macroscopic scales. Ohm's law describes a local and instantaneous relationship between the magnetic field $\boldsymbol{B}$ and the current density in the plasma $\boldsymbol{J}$.

To obtain a non-relativistic MHD model, we will use the laws of classical electrodynamics, we will also use Newton's first law in the form $\rho \dot{\boldsymbol{v}} = \boldsymbol{F}$ and the equation of state given by:

$$\frac{d}{dt}\left(\ln \frac{p}{\rho^{\gamma}}\right) = \eta \frac{\gamma - 1}{p} |\boldsymbol{J}|^2, \tag{1}$$

where $\dot{\boldsymbol{v}}$ is the time-varying velocity, $\boldsymbol{F}$ is a force, η is the resistivity, p is the total pressure, and γ is the adiabatic constant.

In what follows, the MHD equations based on fluid theory and Maxwell's laws are derived.

3.1. Continuity Equation

Consider a fluid element dV with time-varying mass density ρ. The mass change rate $\dot{M}$ describes the mass inflow and outflow through a surface element dS on the boundary of dV.

The mass flux through dS is given by $\rho \boldsymbol{v}$. Thus, considering $d\boldsymbol{S} = \boldsymbol{n} dS$, the total rate of mass flow out of dV is given by the sum of the mass per unit time leaving each face of dV, where the integral is over the surface of dV, that is,

$$\oint_S \rho\, \boldsymbol{v} \cdot \boldsymbol{n}\, dS = -\frac{\partial}{\partial t} \int_V \rho\, dV, \tag{2}$$

where the negative sign in the right-hand term is due to the flux out of the volume. Equation 2 constitutes a conservation law, which guarantees that the rate of change of a quantity contained in V is equal to the flux of that quantity across the boundary of that domain. By Gauss's divergence theorem, we have:

$$\begin{aligned} \frac{\partial}{\partial t} \int_V \rho\, dV &= -\int_V \nabla \cdot (\rho\, \boldsymbol{v})\, dV \\ &\longrightarrow \int_V \left[\frac{\partial \rho}{\partial t} + \nabla \cdot (\rho\, \boldsymbol{v})\right] dV = 0. \end{aligned} \tag{3}$$

For Equation 3 to be satisfied, it is necessary that:

$$\frac{\partial \rho}{\partial t} + \nabla \cdot (\rho\, \boldsymbol{v}) = 0. \tag{4}$$

Equation 4 is called the Continuity Equation and expresses the conservation of mass.

We can express the continuity equation in terms of the total derivative (or Lagrangian derivative) using the relation A.1.1, that is:

$$\frac{d\rho}{dt} = -\rho\nabla\cdot\boldsymbol{v}, \tag{5}$$

where $-\rho\nabla\cdot\boldsymbol{v}$ accounts for the change in ρ that occurs due to the compression ($\nabla\cdot\boldsymbol{v} < 0$) or expansion ($\nabla\cdot\boldsymbol{v} > 0$) of a fluid element. In an incompressible fluid ($\nabla\cdot\boldsymbol{v} = 0$), the variation of mass density is equivalent to the advection of that quantity, since $\frac{d\rho}{dt} = 0$.

3.2. Momentum Equation

Consider a force $\boldsymbol{F}$ per unit volume acting on the fluid elements as a composition of the pressure gradient force (originating from the collective action of particle motion), the Lorentz electromagnetic force, and the gravitational force. Thus, Newton's second law takes the form

$$\rho\frac{d\boldsymbol{v}}{dt} = -\nabla p + \boldsymbol{J}\times\boldsymbol{B} + \rho\boldsymbol{g}. \tag{6}$$

The pressure gradient ∇p has a negative sign because it acts in the direction opposite to the fluid flow. Substituting $\boldsymbol{J}$ with the expression given in Ampère's law and considering $\boldsymbol{B} = \sqrt{\mu_0}\boldsymbol{B}$, we get:

$$\rho\frac{d\boldsymbol{v}}{dt} = -\nabla p + (\nabla\times\boldsymbol{B})\times\boldsymbol{B} + \rho\boldsymbol{g}, \tag{7}$$

which is called the momentum equation of an electromagnetic fluid in its primitive form. On the other hand, MHD numerical simulations use a conservative formulation, so it is necessary to rewrite these equations as conservation laws.

The pressure gradient term in Equation 7 can be rewritten as $\nabla\cdot(p\mathbf{I})$, where $\mathbf{I}$ is the identity matrix, since $\nabla \equiv \nabla\cdot\mathbf{I}$. Using the identities given by Equations A.1.2 and A.1.3, we have:

$$\begin{aligned}\rho\left(\frac{\partial\boldsymbol{v}}{\partial t} + \boldsymbol{v}\cdot\nabla\boldsymbol{v}\right) &= -\nabla\cdot(p\mathbf{I}) \\ &\quad + \nabla\cdot\left(\boldsymbol{B}\boldsymbol{B} - \frac{|\boldsymbol{B}|^2}{2}\mathbf{I}\right) + \rho\boldsymbol{g}.\end{aligned} \tag{8}$$

Substituting Equation 4 into 8 and using the vector identity A.1.1, we obtain:

$$\frac{\partial(\rho\boldsymbol{v})}{\partial t} + \nabla\cdot\left[\rho\boldsymbol{v}\boldsymbol{v} + \left(p + \frac{|\boldsymbol{B}|^2}{2}\right)\mathbf{I} - \boldsymbol{B}\boldsymbol{B}\right] = \rho\boldsymbol{g}, \tag{9}$$

which is defined as the momentum conservation equation.

3.3. Magnetic Induction Equation

In an electrically conductive fluid, current can flow within its domain, so it is possible to relate the current density to an electric field $\boldsymbol{\mathcal{E}}'$ in terms of the electrical resistivity of the fluid η, that is

$$\eta\boldsymbol{J} = \boldsymbol{\mathcal{E}}'. \tag{10}$$

The electric field $\boldsymbol{\mathcal{E}}'$ can be obtained by considering the fluid moving with the plasma mass flow velocity, given by $\boldsymbol{\mathcal{E}}' = \boldsymbol{\mathcal{E}} + \boldsymbol{v}\times\boldsymbol{B}$, that is

$$\eta\boldsymbol{J} = \boldsymbol{\mathcal{E}} + \boldsymbol{v}\times\boldsymbol{B}, \tag{11}$$

which characterizes the resistive Ohm's law. Substituting Equation 11 into Faraday's law and replacing $\boldsymbol{J}$ with the relation given in Ampère's law with $\boldsymbol{B} = \sqrt{\mu_0}\boldsymbol{B}$, we obtain:

$$\frac{\partial\boldsymbol{B}}{\partial t} - \nabla\times(\boldsymbol{v}\times\boldsymbol{B}) = -\nabla\times(\eta\nabla\times\boldsymbol{B}), \tag{12}$$

which is known as the magnetic induction equation.

3.4. Conservation of Energy

The evolutionary equation for energy density is obtained from the equations for pressure, momentum, and magnetic field. The equation of state expresses an evolution characterized by the adiabatic constant γ, relating the mass density and pressure to the current density and resistivity, resulting in:

$$\frac{d}{dt}\ln\left(\frac{p}{\rho^\gamma}\right) = \eta\frac{(\gamma-1)}{p}|\boldsymbol{J}|^2. \tag{13}$$

This is a quasi-isotropic equation due to the contribution of the resistive term on the right-hand side. From it, we can derive the equation that describes the variation of pressure in terms of the variables p, $\boldsymbol{v}$, and $\boldsymbol{B}$.

By simplifying the derivatives on the left side of Equation 13, multiplying it by ρ, and substituting Equation 5 into it, we have:

$$\frac{dp}{dt} - \frac{\gamma p}{\rho}(-\rho\nabla\cdot\boldsymbol{v}) = \eta(\gamma-1)|\boldsymbol{J}|^2. \tag{14}$$

Expanding the terms of $\frac{dp}{dt}$ using the total derivative relation and considering $\gamma p = (\gamma-1)p + p$, we obtain:

$$\frac{\partial p}{\partial t} + \boldsymbol{v}\cdot\nabla p + (\gamma-1)p\nabla\cdot\boldsymbol{v} + p\nabla\cdot\boldsymbol{v} = \eta(\gamma-1)|\boldsymbol{J}|^2. \tag{15}$$

Using Ampère's law in Equation 15, considering $\boldsymbol{B} = \sqrt{\mu_0}\boldsymbol{B}$, we obtain the fluid pressure equation:

$$\frac{\partial p}{\partial t} + \nabla\cdot(p\boldsymbol{v}) + (\gamma-1)p\nabla\cdot\boldsymbol{v} = \eta(\gamma-1)|\nabla\times\boldsymbol{B}|^2. \tag{16}$$

Substituting $p = (\gamma-1)\rho e$ in the first two terms of Equation 16, where e is the internal energy, and dividing through by $(\gamma-1)$, we get:

$$\frac{\partial}{\partial t}(\rho e) + \nabla\cdot(\rho e\boldsymbol{v}) + p\nabla\cdot\boldsymbol{v} = \eta|\boldsymbol{J}|^2. \tag{17}$$

Now, considering the momentum, taking the inner product of $\boldsymbol{v}$ with Equation 7, we get:

$$\begin{aligned}\frac{\partial}{\partial t}\left(\frac{1}{2}\rho|\boldsymbol{v}|^2\right) + \nabla\cdot\left(\frac{1}{2}\rho|\boldsymbol{v}|^2\boldsymbol{v}\right) + \boldsymbol{v}\cdot\nabla p \\ -\boldsymbol{v}\cdot(\boldsymbol{J}\times\boldsymbol{B}) = \rho\boldsymbol{v}\cdot\boldsymbol{g}.\end{aligned} \tag{18}$$

Finally, considering the magnetic field, taking the scalar product of $\boldsymbol{B}$ with Equation 12 and using the vector identities in A.1.4, A.1.5, and A.1.6, we obtain:

$$\begin{aligned}\frac{\partial}{\partial t}\left(\frac{1}{2}|\boldsymbol{B}|^2\right) + \nabla\cdot(\boldsymbol{B}\cdot\boldsymbol{B}\boldsymbol{v} - \boldsymbol{v}\cdot\boldsymbol{B}\boldsymbol{B}) + \boldsymbol{v}\cdot(\boldsymbol{J}\times\boldsymbol{B}) \\ = \nabla\cdot(\boldsymbol{B}\times\eta(\nabla\times\boldsymbol{B})) - \eta|\boldsymbol{J}|^2.\end{aligned} \tag{19}$$

Adding Equations 17, 18, and 19 and substituting $\boldsymbol{J} = \nabla\times\boldsymbol{B}$, we obtain the nearly conservative law that describes the evolution of the energy density given by:

$$\begin{aligned}\frac{\partial E}{\partial t} + \nabla\cdot\left[(E+p)\boldsymbol{v} + \boldsymbol{v}\cdot\left(\frac{|\boldsymbol{B}|^2}{2}\mathbf{I} - \boldsymbol{B}\boldsymbol{B}\right)\right] \\ = \nabla\cdot[\boldsymbol{B}\times\eta(\nabla\times\boldsymbol{B})] + \rho\boldsymbol{v}\cdot\boldsymbol{g}.\end{aligned} \tag{20}$$

3.5. Conservative Ideal MHD

In the case where resistivity is neglected, the resulting model is known as ideal MHD. This model describes the dynamics of an idealized perfectly conducting fluid. Although this represents a significant simplification, it provides a good approximation for highly magnetized plasmas, as such plasmas are often excellent electrical conductors. Therefore, in the ideal MHD model, the resistive terms in the equations for total energy density and magnetic flux are omitted. In its conservative form, the ideal MHD model is given by:

$$\frac{\partial \rho}{\partial t} + \nabla \cdot (\rho \boldsymbol{v}) = 0, \tag{21a}$$

$$\frac{\partial (\rho \boldsymbol{v})}{\partial t} + \nabla \cdot [\rho \boldsymbol{v}\boldsymbol{v} + W\mathbf{I} - \boldsymbol{B}\boldsymbol{B}] = -\rho \nabla \Phi, \tag{21b}$$

$$\frac{\partial \boldsymbol{B}}{\partial t} - \nabla \times (\boldsymbol{v} \times \boldsymbol{B}) = 0, \tag{21c}$$

$$\frac{\partial E}{\partial t} + \nabla \cdot [(E + W)\,\boldsymbol{v} - \boldsymbol{B}(\boldsymbol{v} \cdot \boldsymbol{B})] = -\rho \boldsymbol{v} \cdot \nabla \Phi. \tag{21d}$$

where $W = p + B^2/2$

4. MHD Simulation Methodology

Two jets, flowing in opposite directions, are injected at the center of the domain. Initially, at $t = 0$, there is no magnetic field, and a toroidal magnetic field is introduced along with the jets. The injection region is a cylinder of radius r_j aligned with the y-axis, where the variables are held fixed at their injection values. This region is divided into three parts: a central part where the velocity and magnetic field are zero, and two lateral regions where the jet velocities are opposite, and the magnetic field is reversed between these regions.

To describe the toroidal magnetic field, consider the magnetic field generated by a wire of cross-sectional radius R carrying a current I_0. By applying Ampère's law, the magnetic field inside a radius r is given by:

$$B_t = \begin{cases} \left(\frac{\mu_0 I_0}{2\pi R}\right)\left(\frac{R}{r}\right), & \text{for } r > R, \\ \left(\frac{\mu_0 I_0}{2\pi R}\right)\left(\frac{r}{R}\right), & \text{for } r < R \end{cases} \tag{22}$$

For a jet formed by negative charges, the associated toroidal magnetic field in vector form (referencing the coordinate system in Figure 1b) is:

$$\boldsymbol{B}_t = B_t \left(\frac{y}{r}\hat{i} - \frac{x}{r}\hat{j}\right) \tag{23}$$

These results are consistent with studies such as Rossi et al. Rossi et al. (2017) and Massaglia et al. Massaglia et al. (2019). Building on these findings, we can develop a script and utilize PLUTO, a hydrodynamic code written in C that employs finite elements to integrate the system of differential equations in conservative form Mignone et al. (2007). The numerical simulations follow a methodology similar to that used in the hydrodynamic simulations by Antas et al. (2024), involving a jet entry region in the central domain. This region consists of three computational cells within a Cartesian grid along the x, y, and z directions, with dimensions suited to the source and sufficient to minimize boundary effects.

The initial gas configuration for the simulations is specified by setting the density, thermal pressure, and velocity in each computational cell. We assume an initial static medium ($\boldsymbol{v}(t = 0) = 0$) with density and pressure profiles derived from X-ray data.

5. Relationship Between Structures and the Medium

As the jets emerge from the sphere of influence of the black hole, they interact with the interstellar medium (ISM), leading to a qualitative change in their behavior. The interaction between the jet and the ISM is not fully understood; for instance, the origin of the morphological dichotomy of AGN jets described by Fanaroff and Riley Fanaroff & Riley (1974) remains debated. Fanaroff-Riley type I (FRI) jets typically develop instabilities early and often disrupt the interior of their host galaxy, whereas FRII jets appear well-collimated and propagate stably outside the galaxy. This distinction has significant implications for the host galaxy: FRII jets deposit their energy in external regions without severely impacting the galaxy, while FRI jets inject energy into the galaxy, potentially affecting star formation and gas dynamics. Understanding the stability properties of these jets is therefore crucial.

Figure 2 illustrates how a change in jet power by an order of magnitude leads to a dramatic shift in morphology: more powerful jets maintain stability and escape the galaxy, while less powerful jets become unstable and cause significant distortions within the galaxy, aligning qualitatively with the FRI/II dichotomy.

6. Discussion

The simulations start with the injection of two oppositely directed jets into a central region initially free of magnetic fields, while a toroidal component is introduced together with the jet flow. This configuration isolates the role of the magnetic field in jet stability and reproduces a structured injection region divided into three parts, including a central zone with zero velocity and field and lateral regions with opposite velocities and inverted magnetic fields.

As the jets propagate beyond the black hole's vicinity, their interaction with the ISM becomes decisive. The simulations reproduce the observed Fanaroff–Riley dichotomy: low-power FRI jets develop early instabilities and disrupt the host galaxy's interior, while high-power FRII jets remain collimated and propagate stably into the surrounding medium, influencing the host galaxy on larger scales.

A central result is the correlation between jet power and stability. As illustrated in Fig. 2, increasing the jet power by an order of magnitude shifts the morphology: low-power jets ($\sim 3 \times 10^{43}$ erg s^{-1}) tend to stall and form distorted cavities, whereas high-power jets ($\sim 3 \times 10^{44}$ erg s^{-1}) remain stable, driving strong outflows. This behavior reinforces the physical basis of the FRI/FRII classification.

Environmental conditions also play a key role. Assuming typical cluster parameters—temperature of 2×10^8 K and density profile $\rho_{\rm ICM}(r) = 10^3 \exp[-1.0\,(r/10)^{0.45}]$—the simulations show how density and temperature affect jet propagation. A resolution of 0.25 kpc/cell allows these interactions to be resolved with high accuracy.

Overall, the results clarify the physical processes shaping radio structures such as jets, lobes, and plumes. By connecting jet stability to magnetic fields, power, and environmental conditions, these simulations refine theoretical models of radio galaxies and contribute to a broader understanding of plasma physics, high-energy astrophysics, and extragalactic evolution.

7. Conclusion

In deriving the conservative MHD equations based on fluid theory and Maxwell's equations, the goal was to understand the

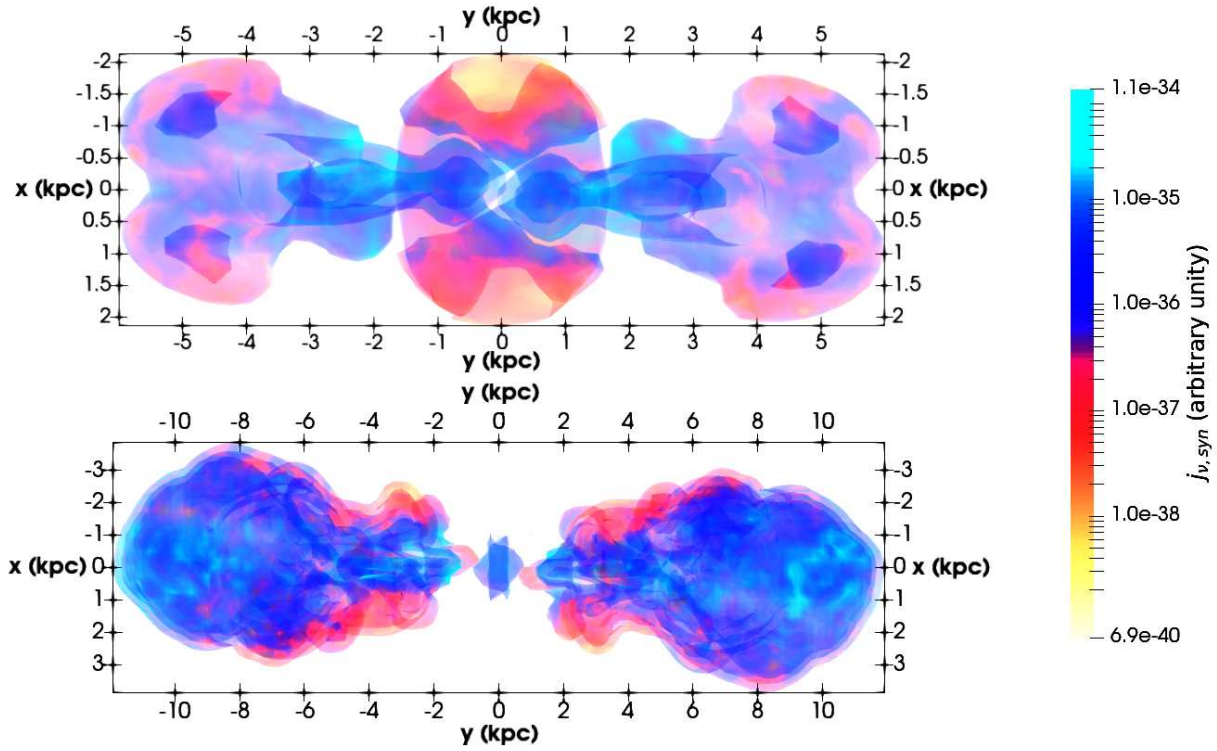

Figure 2. (a) Low-power AGN jets (approximately 3×10^{43} ergs/s) succumb to global magnetic instabilities, stall within their host galaxies, and create cavities with noticeable distortions. (b) High-power jets (approximately 3×10^{44} ergs/s) remain stable, exit their host galaxies, and generate strong outflows. The evolution period for the structures was 8 Myr with an adopted magnetic field strength of approximately 10^{-5} G. The medium conditions in these simulations follow typical cluster distributions, with a temperature of about 2×10^8 K and medium density ρ_{ICM} following a spherical distribution given by $\rho_{ICM}(r) = 10^3 \times \exp(-1.0 \times (r/10)^{0.45})$. The resolution adopted is 0.25 kpc/cell.

fundamental physical mechanisms governing the formation, evolution, and interaction of these jets with the intergalactic medium. A brief demonstration of the methodology was provided, analyzing the interaction between the jets and the medium, allowing us to consider the morphological dichotomies observed in jets from active galactic nuclei (AGN). This demonstration indicates that variations in jet power lead to qualitative changes in morphology, with more powerful jets exhibiting greater stability compared to less powerful ones. This observation aligns with the FRI/FRII dichotomy and highlights the importance of understanding jet stability and its impact on the dynamics of the host galaxy.

Through these simulations, we gained a deeper understanding of the underlying physical processes and their relationship to observational phenomena. Additionally, this methodology contributes to the development of more accurate theoretical models that not only deepen our understanding of radio galaxy physics but also have broader implications for astrophysical phenomena on various scales.

Acknowledgements. The authors acknowledge the National Laboratory for Scientific Computing (LNCC/MCTI, Brazil) for providing HPC resources of the SDumont supercomputer, which have contributed to the research results reported within this paper. URL: `http://sdumont.lncc.br`. ASRA also acknowledge the financial support from Conselho Nacional de Desenvolvimento Científico e Tecnológico CNPq.

References

Antas A. S. R., Caproni A., Machado R. E. G., Laganá T. F., Souza G. S., 2024, MNRAS, 533, 1341
Antonucci R., 1993, ARA&A, 31, 473
Blandford R. D., Znajek R. L., 1977, MNRAS, 179, 433
Blandford R. D., Payne D. G., 1982, MNRAS, 199, 883
Burbidge G. R., 1956, ApJ, 124, 416
Fanaroff B. L., Riley J. M., 1974, MNRAS, 167, 31P
Massaglia S., Bodo G., Rossi P., Capetti S., Mignone A., 2019, A&A, 621, A132
Mignone A., Bodo G., Massaglia S., Matsakos T., Tesileanu O., Zanni C., Ferrari A., 2007, ApJS, 170, 228
Netzer H., 2015, ARA&A, 53, 365
Rossi P., Bodo G., Capetti A., Massaglia S., 2017, A&A, 606, A57
Salpeter E. E., 1964, ApJ, 140, 796
Scheuer P. A. G., 1974, MNRAS, 166, 513
Schmidt M., 1963, Natur, 197, 1040
Tchekhovskoy A., 2015, ASSL, 414, 45
Urry C. M., Padovani P., 1995, PASP, 107, 803

Appendix A: Identities

This appendix presents the vector identities used throughout this work. Let f be a real function and a, b, c be vectors, all differentiable with respect to x, y and z.

$$\nabla \cdot (f\boldsymbol{a}) = f\nabla \cdot \boldsymbol{a} + \boldsymbol{a} \cdot \nabla f, \tag{A.1a}$$
$$\boldsymbol{a} \times (\nabla \times \boldsymbol{b}) = (\nabla \boldsymbol{b}) \cdot \boldsymbol{a} - \boldsymbol{a}\nabla \cdot \boldsymbol{b}, \tag{A.1b}$$
$$\nabla \cdot (\boldsymbol{a}\,\boldsymbol{b}) = \boldsymbol{a} \cdot \nabla \boldsymbol{b} + \boldsymbol{b}\nabla \cdot \boldsymbol{a}, \tag{A.1c}$$
$$\nabla \cdot (\boldsymbol{a} \times \boldsymbol{b}) = \boldsymbol{b} \cdot \nabla \times \boldsymbol{a} - \boldsymbol{a} \cdot \nabla \times \boldsymbol{b}, \tag{A.1d}$$
$$\boldsymbol{a} \cdot (\boldsymbol{b} \times \boldsymbol{c}) = \boldsymbol{c} \cdot (\boldsymbol{a} \times \boldsymbol{b}) = \boldsymbol{b} \cdot (\boldsymbol{c} \times \boldsymbol{a}), \tag{A.1e}$$
$$(\boldsymbol{a} \times \boldsymbol{b}) \times \boldsymbol{c} = \boldsymbol{a} \cdot \boldsymbol{b}\boldsymbol{c} - \boldsymbol{b} \cdot \boldsymbol{c}\boldsymbol{a}, \tag{A.1f}$$
$$\nabla \times (\boldsymbol{a} \times \boldsymbol{b}) = \nabla \cdot (\boldsymbol{b}\boldsymbol{a} - \boldsymbol{a}\boldsymbol{b}). \tag{A.1g}$$